Two-dimensional kinetic simulation of electrostatic instabilities in a Hall plasma.

IEPC-2022-314

Presented at the 37th International Electric Propulsion Conference
Massachusetts Institute of Technology, Cambridge, MA, USA
June 19-23, 2022

E. Bello-Benítez[1], A. Marín-Cebrián, J.J. Ramos and E. Ahedo.
Equipo de Propulsión Espacial y Plasmas, Universidad Carlos III de Madrid, Leganés, 28911, Spain

The problem of anomalous transport in partially magnetized $\boldsymbol{E}_0 \times \boldsymbol{B}_0$ plasmas, such as the Hall thruster discharge, remains still unsolved. In this context, the electron cyclotron drift instability (ECDI) has been considered as a possible candidate triggering azimuthal oscillations that result in cross-field electron transport. In this article, we further explore this instability by revisiting the linear kinetic theory and through nonlinear particle-in-cell simulations with a recently developed in-house 2D electrostatic code. A simplified scenario on a periodic plasma starting from homogeneous equilibrium conditions is able to reproduce the growth and saturation stages of the ECDI, that lead, indeed, to an anomalous electron current. However, in the long term, oscillations vanish and so it does the electron cross-field axial transport. Then, instead a fully periodic plasma, injection conditions through the axial boundaries are explored. We distinguish several regimes depending on the ion residence time compared with the saturation time of the ECDI. When this two are similar, the plasma is able to hold a stationary azimuthal oscillation that carries an electron cross-field transport.

I. Introduction

The problem of anomalous electron cross-field transport remains as one of big open challenges for the community of $\boldsymbol{E}_0 \times \boldsymbol{B}_0$ plasmas. In the field of plasma propulsion, this problem has been mainly studied in the context of Hall-thruster discharges and represent one big obstacle on the way towards to predictive efficient numerical models. The large drift of electrons in the azimuthal direction of the Hall thruster is a source of several families of azimuthal oscillations that are potential candidates to explain the anomalous transport and have been observed experimentally [1–6]. The classical explanation [7] for the impact of oscillations on transport relies on the correlation of oscillations in density and electric field in the $\boldsymbol{E}_0 \times \boldsymbol{B}_0$ direction under the presence of a magnetic field.

The amount of articles devoted to the analysis of instabilities and turbulence in Hall thrusters is extensive. With a macroscopic description for ions and electrons, some of the authors of this article have conducted global [8] and local [9] linear stability analyses. In these references two-stream, drift-gradient and drift-dissipative instabilities are discussed. Similar recent studies by other authors are [10–14].

When using a kinetic formulation for the electrons, the analytical studies of instabilities is usually limited to a homogeneous and collisionless plasma. For the conditions of a Hall thruster, where electrons are magnetized but ions are not, the dispersion relation of the electron cyclotron drift instability (ECDI) is obtained[15, 16]. This classical instability have been revisited, during the last two decades, by several authors [17–21], in the context of Hall thrusters. Also from the point of view of kinetic simulations [17, 22–26] and experiments [4–6, 27].

[1]ebello@ing.uc3m.es

Kinetic models aimed to analyze electron turbulence and anomalous transport in the plane perpendicular to $\boldsymbol{B}_0$ can be classified in 1D azimuthal[22, 25, 26] and 2D axial-azimuthal [17, 23, 24]. The latter case has been the subject of a recent benchmark by several groups [28]. Many 2D simulations include a number of phenomena that makes challenging to compare the results with the ECDI linear theory; such as, inhomogeneous magnetic field, collisions, ionization or electrical connection between anode and cathode. The 1D simulations are closer to the linear theory of the ECDI but they still add effects that are not considered in the dispersion relation, such as refreshing of particle velocities or collisions.

In this work, we revisit in section II the linear theory of the ECDI in the limit of perpendicular propagation. Then, in section III, we present a recently developed in-house two-dimensional particle-in-cell (PIC) code that is intended to be used in the simulation of electrostatic instabilities in $\boldsymbol{E}_0 \times \boldsymbol{B}_0$ plasmas. The numerical model is used in section IV to simulate the ECDI in a periodic plasma starting from equilibrium conditions and with an uniform magnetic field $\boldsymbol{B}_0$ perpendicular to the domain. From analogy with a Hall thruster geometry, this is the axial azimuthal plane. This simulation setup is intended to comply exactly with the assumptions used in the derivation of the ECDI dispersion relation. Indeed, the ECDI develops but oscillations vanish in the long term. In section V, axial periodic conditions are modified by injection surfaces at fixed electric potential. Different behaviors are identified depending on the value of the ion residence time relative to the characteristic saturation time of the ECDI.

II. Linear theory of the electron-cyclotron drift instability

The propagation of waves is studied in a homogeneous equilibrium plasma subjected to mutually perpendicular magnetic[a] $\boldsymbol{B}_0 = B_0\mathbf{1}_x$ and electric $\boldsymbol{E}_0 = E_0\mathbf{1}_z$ fields. From analogy with a Hall-thruster geometry, let us refer to the directions of $\boldsymbol{B}_0$, $\boldsymbol{E}_0$ and $\boldsymbol{E}_0 \times \boldsymbol{B}_0$ as radial (x), axial (z) and azimuthal (y). Electrons are considered magnetized and having a drifting Maxwellian velocity distribution function (VDF) with mean velocity $\boldsymbol{u}_{e0} = u_{ye0}\mathbf{1}_y$ and temperature T_{e0}. The electron mean velocity is the result of the $\boldsymbol{E}_0 \times \boldsymbol{B}_0$ drift, so that $u_{ye0} = E_0/B_0$. On the other hand, ions have velocity $\boldsymbol{u}_{i0} = u_{zi0}\mathbf{1}_z$ and are assumed cold and unmagnetized; that is, they do not feel $\boldsymbol{B}_0$. Implicitly, this means that ions must also disregard the $\boldsymbol{E}_0$ so that an homogeneous equilibrium is feasible. For these conditions, coming from the perturbed Vlasov equation, the electron density perturbation is given by

$$\frac{n_{e1}}{n_0} = \left[1 + \sum_{m=-\infty}^{\infty} \frac{\omega_e \exp(-b_e) I_m(b_e)}{\sqrt{2}k_\parallel c_e} Z\left(\frac{\omega_e - m\omega_{ce}}{\sqrt{2}k_\parallel c_{e0}}\right)\right] \frac{e\phi_1}{T_{e0}}, \tag{1}$$

being n_0 the equilibrium quasineutral plasma density, $\omega_e = \omega - k_y u_{ye0}$ the electron Doppler-shifted frequency, $\omega_{ce} = eB_0/m_e$ the cyclotron frequency, $b_e = k_\perp^2 \rho_{e0}^2$, $\rho_{e0} = c_{e0}/\omega_{ce}$ the electron Larmor radius, $c_{e0} = \sqrt{T_{e0}/m_e}$ the electron thermal velocity, $k_\perp$ the wavevector component perpendicular to $\boldsymbol{B}_0$, $k_\parallel$ the parallel one, I_m the modified Bessel functions of the first kind and Z the plasma dispersion function. The perpendicular propagation limit $k_\parallel = 0$, we are interested in, yields

$$\frac{n_{e1}}{n_0} = \left[1 - \exp(-b_e) I_0(b_e) + 2\omega_e^2 \exp(-b_e) \sum_{m=1}^{\infty} \frac{I_m(b_e)}{\omega_e^2 - m^2\omega_{ce}^2}\right] \frac{e\phi_1}{T_{e0}}. \tag{2}$$

On the other hand, the ion perturbations, from a cold fluid model, follow the expression

$$\frac{n_{i1}}{n_0} = \frac{k^2 c_{s0}^2}{\omega_i^2} \frac{e\phi_1}{T_{e0}} \tag{3}$$

with k the magnitude of the wavevector $\boldsymbol{k}$, $\omega_i = \omega - k_z u_{zi0}$ the ion Doppler-shifted frequency and $c_{s0} = \sqrt{T_{e0}/mi}$ the sound speed. Using expressions (2) and (3), together with the linearized Poisson equation, gives the two-dimensional dispersion relation

$$1 + k^2\lambda_{D0}^2 = \frac{k^2 c_{s0}^2}{\omega_i^2} + \exp(-b_e) I_0(b_e) + 2\omega_e^2 \exp(-b_e) \sum_{m=1}^{\infty} \frac{I_m(b_e)}{\omega_e^2 - m^2\omega_{ce}^2}. \tag{4}$$

[a] Subindex '0' stands for equilibrium conditions everywhere in the article.

Here, we have a resonance when ω_e is close to a cyclotron harmonic $m\omega_{ce}$. This dispersion relation is solved for the complex frequencies $\omega = \omega_r + j\gamma$ with all other parameters fixed, including $\boldsymbol{k}$. An alternative form of writing equation (4) comes from isolating ω_i, that leads to the following expression for one of the modes:

$$\omega_i = \pm \frac{k c_{s0}}{\sqrt{1 + k^2 \lambda_{D0}^2 - g(\omega_e)}}, \tag{5}$$

where $-g(\omega_e)$ gathers the electron Bernstein terms in the right-hand side of equation (4). This form of the dispersion relation is the basis for numerically solving the unstable mode of the ECDI relation in reference [19], which is the approach also followed here. Equation (5) reminds of an ion-acoustic wave with, in the denominator, a non-neutral correction $k^2\lambda_D^2$ and the resonant destabilizing term $g(\omega_e)$. Therefore, the unstable scales tend to concentrate in narrow bands near the resonances. This behavior is characteristic of the ECDI in the perpendicular propagation limit.

The unstable solution of equation (4) for an infinite plasma is shown in figure 1 for $k_z = 0$; and equilibrium conditions $n_0 = 10^{17}$ m^{-3}, $u_{zi0} = 5$ km/s, $u_{ye0} = 250$ km/s, $T_{e0} = 2$ eV, $B_0 = 200$ G. The finite plasma dispersion relation is of interest when considering the simulation results and leads to a discrete spectrum with the reproduced scale being $k_y = n2\pi/L_y$. The results here are for $L_y = 2.6793$ mm. This the azimuthal domain size used in simulations shown in the coming sections. This solution is for Hydrogen ions. This decision is based on speeding up simulations. Since the characteristic frequencies and growth rates of the ECDI approximately scale with $1/\sqrt{m_i}$.

In this solution the characteristic resonant behavior of the ECDI can be observed. For this case, the fastest growing modes take place close to $m = 1$ and $m = 2$ (being $m = 1$ slightly dominant). The $m = 1$ mode from the discrete discrete dispersion relation has $n = 7$, frequency $\omega_r = 35.4$ MHz, azimuthal wavelength $\lambda_y = 0.38$ mm and phase velocity $\omega_r/k_y = 13.5$ km/s. The $m = 2$ mode from the discrete dispersion relation has $n = 13$, frequency $\omega_r = 53.8$ MHz and azimuthal wavelength $\lambda_y = 0.21$mm. These frequencies are, approximately, one order of magnitude higher than those expected in Xenon. An important feature of the ECDI is that, usually, ω_r and γ have comparable magnitudes, making difficult to differentiate a linear stage in nonlinear simulations.

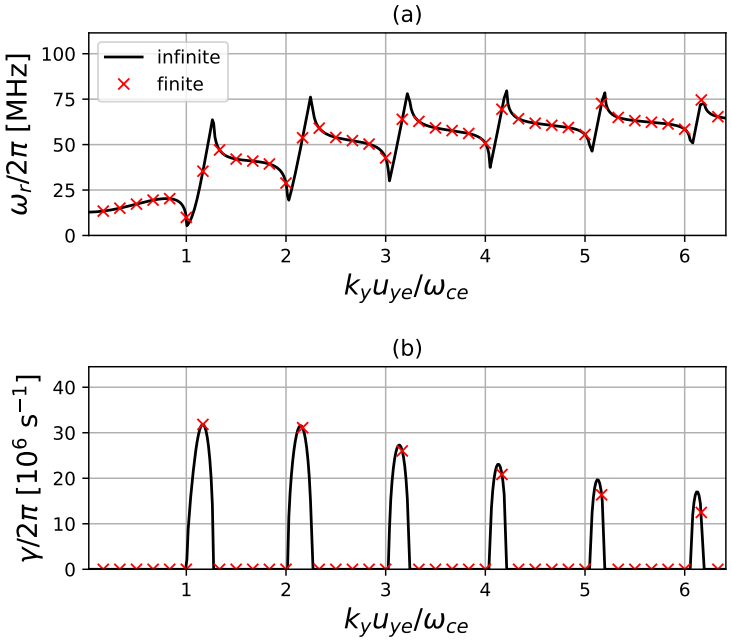

Fig. 1 ECDI dispersion relation for Hydrogen ions ($m_i = 1.6726 \times 10^{-27}$ kg) with $k_\parallel = 0$ and $k_z = 0$; with equilibrium conditions $n_0 = 10^{17}$ m^{-3}, $u_{zi0} = 2.5$ km/s, $u_{ye0} = 250$ km/s, $T_{e0} = 2$ eV, $B_0 = 200$ G. Black solid line is the solution for an infinite plasma. Red crosses stand for the solution in a finite plasma with $L_y = 2.6793$ mm.

III. Electrostatic particle-in-cell model

To simulate and analyse instabilities and electron transport on a Hall plasma, a recently developed in-house 2D particle-in-cell (PIC) code and Poisson solver are used. Both modules are coded in Fortran and use OpenMP parallelization capabilities. The Poisson solver uses internally the external libraries LIS (for linear system solution) and FFTW3 (for Fourier-transform operations). Our PIC code has been conceived as a flexible tool for simulating a diversity of plasma-discharge scenarios. One of the primary goals of the code is the analysis of Hall-thruster anomalous transport and instabilities in the axial-azimuthal plane (after previous efforts with fluid models [8, 9]).

The motion of particles is solved numerically by using an standard Boris method. The Poisson solver uses different schemes depending on boundary conditions. If Neumann or Dirichlet conditions are used for one or more boundaries, the solver uses a second order finite difference scheme for the Laplace operator and electric field. The final linear system of equations governing the electric potential is solved with the LIS library. When all boundaries are periodic, spectral methods are used to easily solve the Poisson equation in the Fourier complex space. The Fourier transform and the inverse operation are performed with the FFTW3 library. In this latter case a zero average potential is imposed. Finite difference methods have been tested on periodic domains, imposing a reference potential on an arbitrary single node, producing sometimes spurious local behavior close to the reference-potential point that can ruin the simulation.

One of the objectives of this work is the simulation of the ECDI in an homogeneous plasma with assumptions as close as possible to those used in the theoretical derivation of the dispersion relation (4). Electron and singly-charged ion species are considered and treated with a PIC formulation. Particles of both species are considered with equal and constant weights. In order to comply with the hypothesis in section II, electron and ion particles are moved with electric fields $\boldsymbol{E}_e = \boldsymbol{E}_0 + \boldsymbol{E}_1$ and $\boldsymbol{E}_i = \boldsymbol{E}_1$, respectively; being $\boldsymbol{E}_0 = E_0\ \mathbf{1}_z$ an equilibrium uniform value and $\boldsymbol{E}_1$ the local fluctuation relative to $\boldsymbol{E}_0$ that comes as solution to the Poisson equation. In addition, electron motion account also for a magnetic field $\boldsymbol{B}_0 = B_0\ \mathbf{1}_x$ perpendicular to the simulation plane. That is to say, ions react only to the fluctuating part of the electric field. Collisions are disregarded.

At the beginning of the simulation, both species are loaded homogeneously with equal densities n_0. Ions are generated with no temperature and velocity $\boldsymbol{u}_i = u_{zi0}\ \mathbf{1}_z$. Electron particle velocities are sampled from a drifting Maxwellian

$$f_e(\boldsymbol{v}) = n_0 \left(\frac{m_e}{2\pi T_{e0}}\right)^{3/2} \exp\left[-\frac{m_e(\boldsymbol{v}-\boldsymbol{u}_{e0})\cdot(\boldsymbol{v}-\boldsymbol{u}_{e0})}{2T_\alpha}\right], \tag{6}$$

with temperature T_{e0} and mean velocity $\boldsymbol{u}_e = u_{ye0}\ \mathbf{1}_y$, where $u_{ye0} = E_0/B_0$ is the $\boldsymbol{E}_0 \times \boldsymbol{B}_0$ drift. The properties of the initial populations correspond to a homogeneous equilibrium state. The evolution observed in subsequent times is a consequence of plasma instabilities. The results shown in this work apply a moving average to the results in a time window that coincides with Δt_{print}. This is done to mitigate the level of noise and it has been carefully checked that averaged results are representative of the instantaneous behavior.

Regarding boundary conditions, two types of simulations are shown in this article: (i) periodic plasma and (ii) axial injection with azimuthal periodic conditions. More details about the boundary conditions are given in the corresponding section.

IV. ECDI simulation in homogeneous equilibrium

In this section, results are shown for an EDCI simulation in a periodic plasma, starting from a homogeneous equilibrium. Periodic conditions are applied to, both, particles and electric field. Figure 2 summarizes the simulation setup. Let us remind that, to comply with assumptions behind the ECDI theory, the electric field depends on the species. The fluctuating part comes from the Poisson solution. The decision on ions not reacting to $\boldsymbol{E}_0$ allows to disregard ion acceleration and the consequent axial inhomogeneity that is not accounted for in the ECDI theory. Moreover, ion acceleration is not consistent with axial periodic conditions and the treatment of ions have been seen to be troublesome in 1D-y simulations [22, 26]. The solution for the electric potential ϕ and field $\boldsymbol{E}_1 = -\nabla\phi$ uses the spectral version of the Poisson numerical code. Because of periodic boundary conditions, the number of particles in the domain remains constant. Moreover, the number of electron and ion particles coincide so that the net charge in the domain is zero.

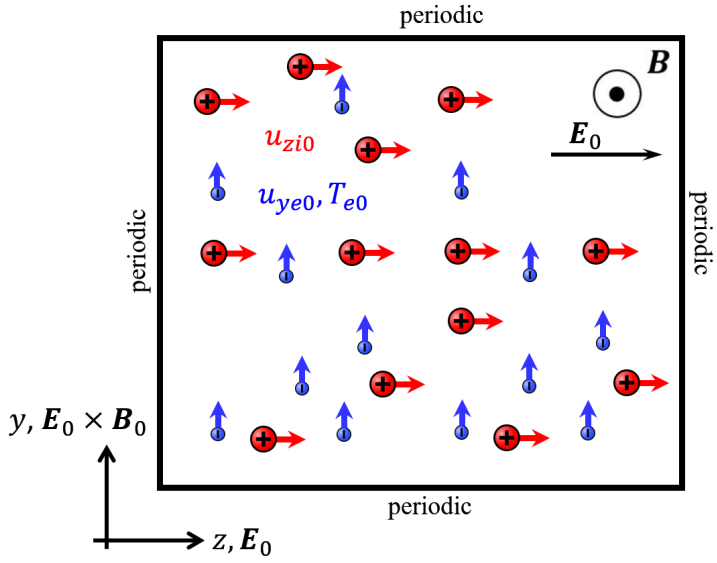

Fig. 2 Diagram summarizing the simulation axes, boundary conditions and initial equilibrium state for the periodic ECDI simulation.

The physical and numerical parameters of the PIC simulation are summarized in tables 1 and 2, separating fundamental ones in (a) from derived values in (b) that are included to give the main characteristic lengths, frequencies and velocities of the system. The main features of this simulation have been already described. Other than already said, a square domain is used with L_y long enough to properly capture the largest scale of the ECDI, close to the resonance $m = 1$. This is demonstrated by the discrete spectrum in figure 1.

Table 1 Physical parameters of the homogeneous ECDI simulation. Apart from paramters defined in the main text, ρ_{e0} is the electron Larmor radius, $c_{e0} = \sqrt{T_{e0}/m_e}$ is the electron thermal speed, $\omega_{Pe0} = \sqrt{e^2 n_0/\varepsilon_0 m_e}$ and $\omega_{Pi0} = \sqrt{e^2 n_0/\varepsilon_0 m_i}$ are, respectively, the electron and ion plasma frequencies; and $\omega_{lh} = eB_0/\sqrt{m_i m_e}$ is the lower-hybryd frequency.

(a) Fundamental

L_y [mm]	2.6793
L_z [mm]	2.6793
E_0 [V/m]	5×10^3
B_0 [G]	200
m_i [u]	1
n_0 [m^{-3}]	1×10^{17}
u_{zi0} [km/s]	2.5
T_{e0} [eV]	2

(b) Derived

Lengths	
λ_{D0} [μm]	33.3
ρ_{e0} [μm]	169
Velocities	
u_{ye0} [km/s]	250
c_{e0} [km/s]	593
c_{s0} [km/s]	13.8
Frequencies	
ω_{Pe0} [GHz]	2.84
ω_{ce} [GHz]	0.560
ω_{Pi0} [MHz]	66.3
ω_{lh} [MHz]	13.1

Table 2 Numerical physical and numerical parameters of the homogeneous ECDI simulation. $N_{y,z}$ are the number of nodes in y and z directions, N_{ppc} is the initial number of particles per cell, Δt is the simulation time step, N_t is the number of time steps, Δt_{print} is diagnostics print-out time, Δy and Δz are the grid spacing in y and z directions; and $\omega_{\max}$ is the maximum frequency that can be measured according to Δt_{print}

(a) Fundamental

N_y	83
N_z	83
N_{ppc}	100
Δt [s]	5×10^{-12}
N_t	6×10^{5}
Δt_{print} [s]	1×10^{-9}

(b) Derived

Lengths	
Δy [μm]	32.7
Δz [μm]	32.7
Frequencies	
$\omega_{\max}$ [GHz]	1.0

The evolution in the yz-plane of E_y is represented in figure 3 for several times. In figure 4, the evolution in the yt-plane and zt-plane is plotted for fixed $z = 5L_z/6$ and $y = L_y/2$, respectively The initial equilibrium state is unstable because of the ECDI, so that any perturbations in initial population start to grow. The oscillatory field has a growing amplitude until $t \approx 0.3$ μs, where saturation of the instability seems to happens. For times after before 0.3 μs there is little mix of modes and we can detect a quite monochromatic wave with clearly identifiable λ_y and ω_r. The propagation of this wave is mainly azimuthal and happens in the $+\boldsymbol{E}_0 \times B_0$ direction. For times after 0.3 μs, there seems to be a significant mixing of modes, that can be better observed in figure 3, starting on $t = 0.5$ μs. For subsequent times the oscillations are damped out and the plasma seem to tend to an equilibrium state that is different from the initial one.

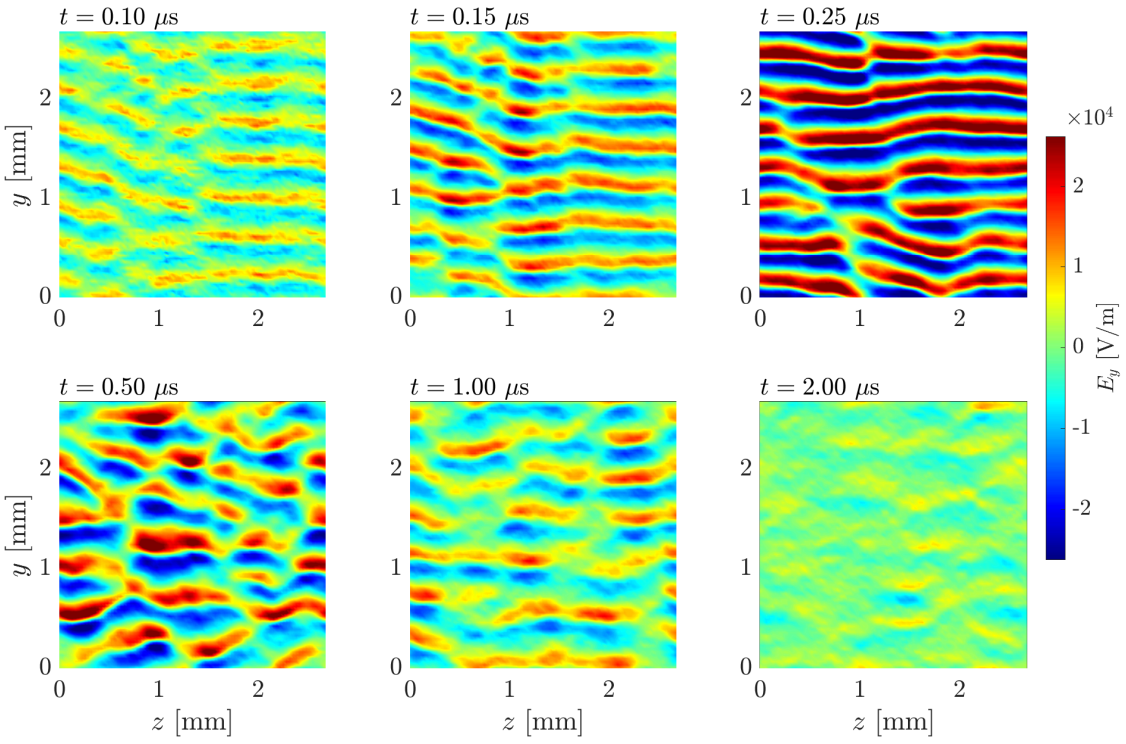

Fig. 3 Time evolution of E_y in the yz-plane, for periodic boundary conditions and parameters in tables 1 and 2.

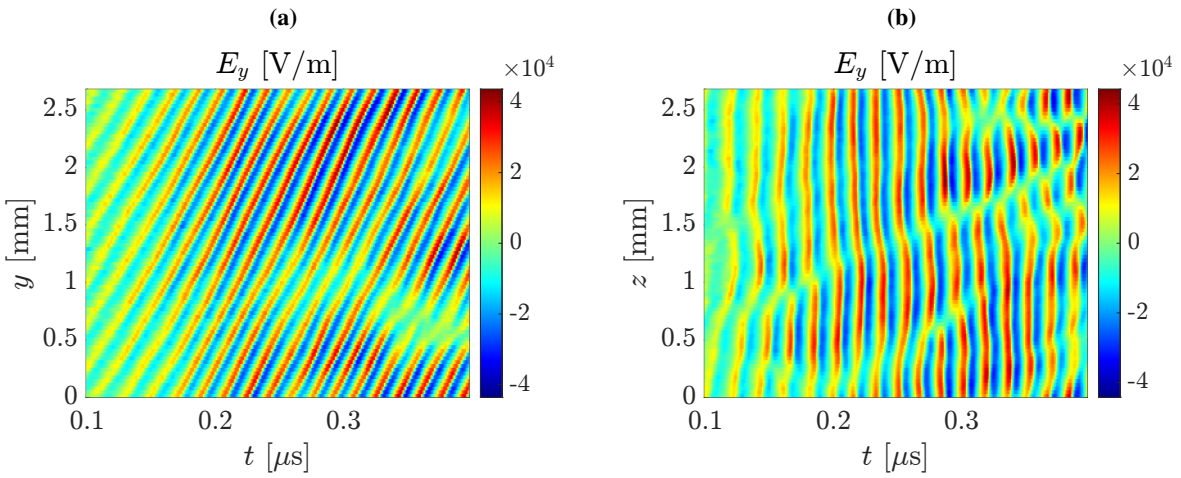

Fig. 4 Evolution of E_y in the (a) yt-plane for fixed $z = 5L_z/6$ and (b) zt-plane for fixed $y = L_y/2$.

The saturation and post-saturation evolution of E_z and other plasma properties are represented in figures 5 and 6. Let us focus in the saturation behavior for now. Looking at E_z, we emphasize again that the instability is mainly azimuthal, what is translated into a milder and more disordered E_z than E_y. However, there are some two-dimensional axial effects that perturb the plasma. The oscillatory behavior of the instability can be also seen in the densities n_i and n_e that then to follow the electric field wave. The peaks of n_i are more prominent that n_e. Even if ions are heavier than electrons, they are not magnetized and are more easily trapped in the potential wave. The n_e space evolution tends to follow n_i because of the natural tendency of the plasma to locally satisfy quasineutrality, but electrons are not so so easily trapped because of the magnetic confinement. A visible oscillation develops also in the ion azimuthal macroscopic velocity u_{yi}, electron temperature T_e and, to a lesser extent, in T_i.

In the post-saturation state, there is a diminishing of the electric field and oscillations seem to dampen. The plasma properties seem to converge to a new steady state that is fairly homogeneous. The average densities n_e and n_i are, of course, equal to the initial state since the number of particles in the simulation does not change. However, other properties related to higher-order moments of the VDF, such as u_{yi}, T_i and T_e, are modified. Since ions are trapped by the wave, while the ECDI grows, they develop an azimuthal average velocity. One of the effects of the instability is also the significant heating of, both, electron and ions. Looking at the macroscopic properties, it is clear that the final state of the populations is much more energetic than the initial equilibrium. Energy conservation is discussed in a coming subsection.

The electron and ion heating is also evident when looking at VDF and particles in phase space. Figure 7 plots the initial and final 1D-VDF of electrons measured at the central point of the domain. We see that the initial electron population perfectly matches a drifting Maxwellian VDF, as it should. At the end of the simulation the dispersion in the electron velocities is much higher and seem to fairly isotropic. The reconstructed VDFs seem to depart from a Maxwellian, but this should be checked with improved statistics. The evolution of ion particles in the phase space is plotted in figure 8. We see that the initial cold population evolves towards the formation of vortex-like structures in the v_y-y plane when close to the saturation. This type of behavior is characteristic of ion-wave trapping and has been already seen in other works [22, 26]. After saturation, the vortices are distorted and destroyed but the distribution function of v_y keeps a one-sided long tail. Ions are noted to play an important role in the formation and saturation of the ECDI. In the plane v_z-z, there is a clear ion heating and the distribution function of v_z, in contrast to v_y, has a more conventional shape with symmetric tails.

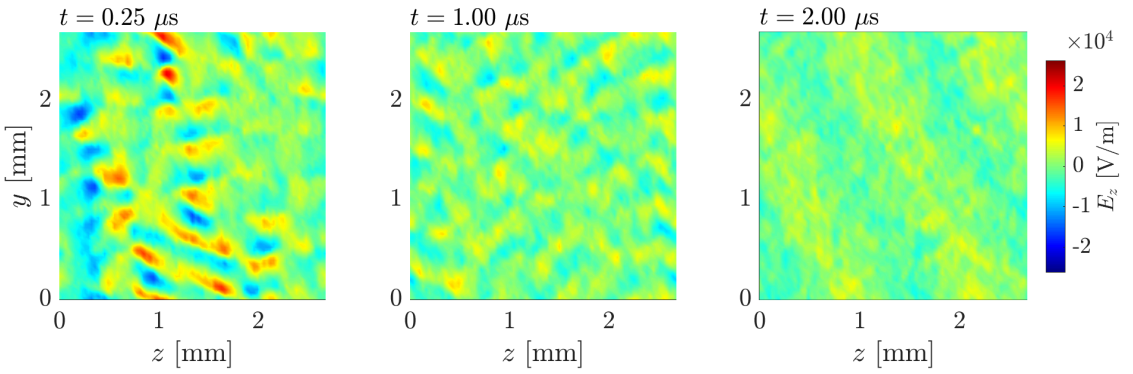

(a) E_z

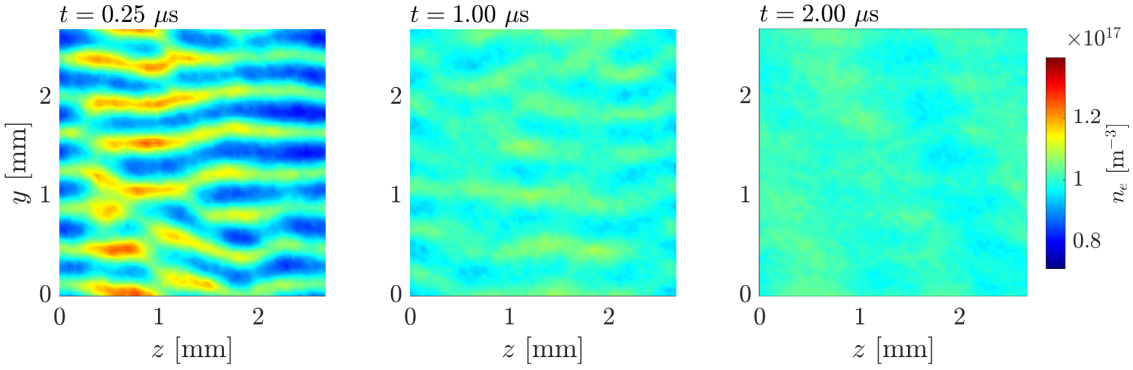

(b) n_e

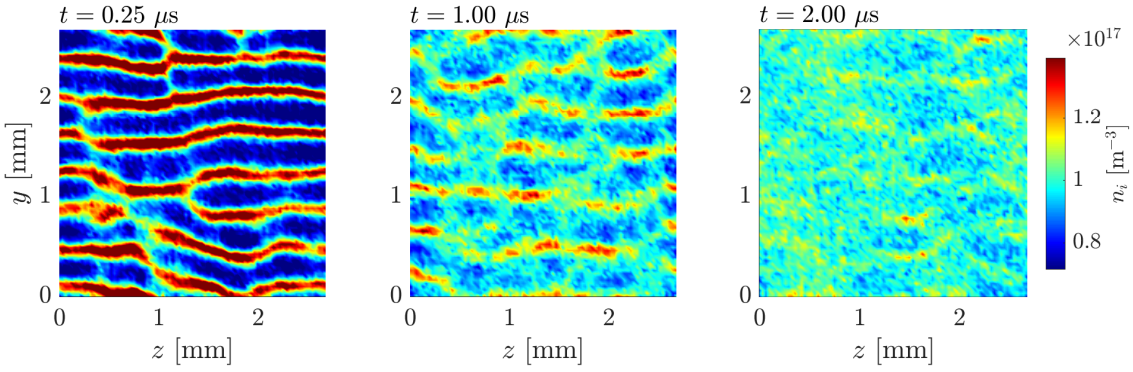

(c) n_i

Fig. 5 Time evolution of E_z, n_e and n_i in the yz-plane.

These results do not match the behavior reported in other 1D-y [22, 25, 26] and 2D-zy [17, 23, 24, 28], where the plasma and electric field hold sustained oscillations that do not vanish with time. Regarding the comparison of existing 2D models with our simulations here, it is not trivial since references [17, 23, 24, 28] account for other effects, such as inhomogeneous magnetic field, anode-cathode circuit, ionization or collisions. Here we disregard many of these effects, since our goal is to get as close as possible to the hypotheses of the ECDI linear theory. A fairer comparison is that with the 1D-y models [22, 25, 26]. Regarding the ion treatment, the works [22, 26] account for a fake axial dimension and the acceleration of the ions due to $\boldsymbol{E}_0$. Because ions are accelerated, periodic axial conditions would lead to a forever growing axial velocity. In order to solve this issue, particles that leave the domain

through axial boundaries are re-injected with a refreshed velocity. This is, particles that have interacted with the electrostatic wave and have a modified VDF (see figures 7 and 8) are removed from the simulation and substituted by particles with the initial VDF. Therefore, the re-injection conditions could have a strong interaction with the instability. Our approach is different and we cope with ion acceleration, and the resultant axial inhomogeneity, by disregarding $\boldsymbol{E}_0$ on the ion motion. Since ions move only according to the electric field fluctuation $\boldsymbol{E}_1$, periodic conditions can be applied, not only azimuthally, but also axially. Because there is no change in velocity for particles going through boundaries, the change in the VDF of ions and electrons from the initial one is solely a result of the instability.

Although our simulation of a periodic plasma does not lead, in the long term, to a sustained oscillation, it can still offer a valuable physical insight on the ECDI behavior and the influence on electron transport. Several aspects are discussed in the next subsections.

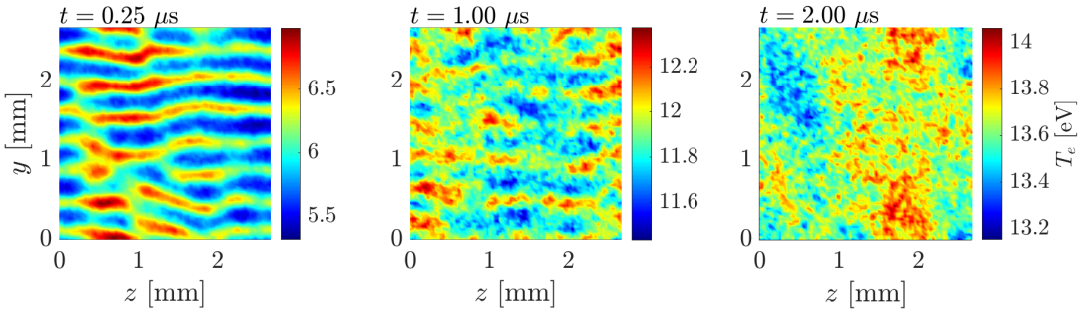

(a) T_e

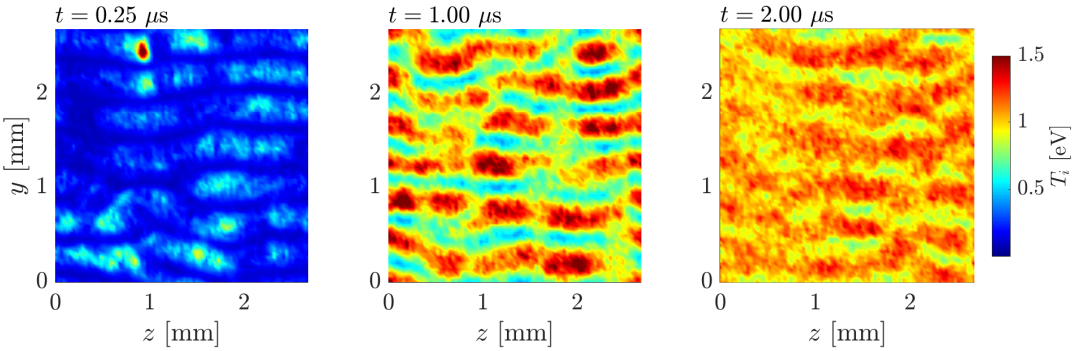

(b) T_i

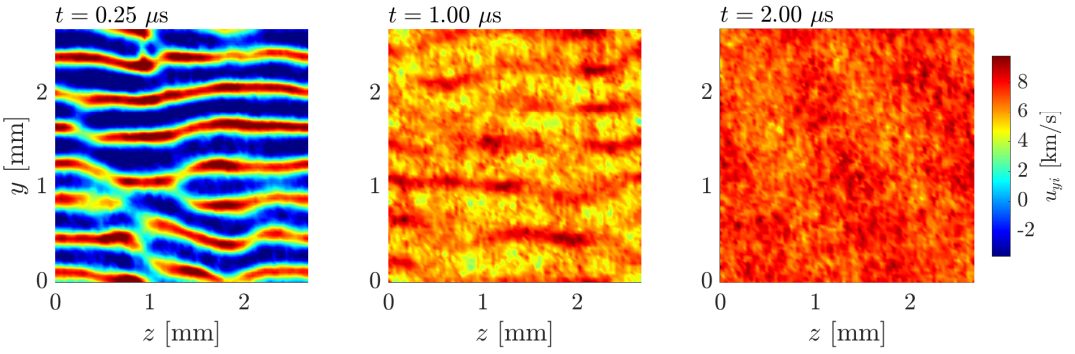

(c) u_{yi}

Fig. 6 Time evolution of T_e, T_i and u_{yi} in the yz-plane.

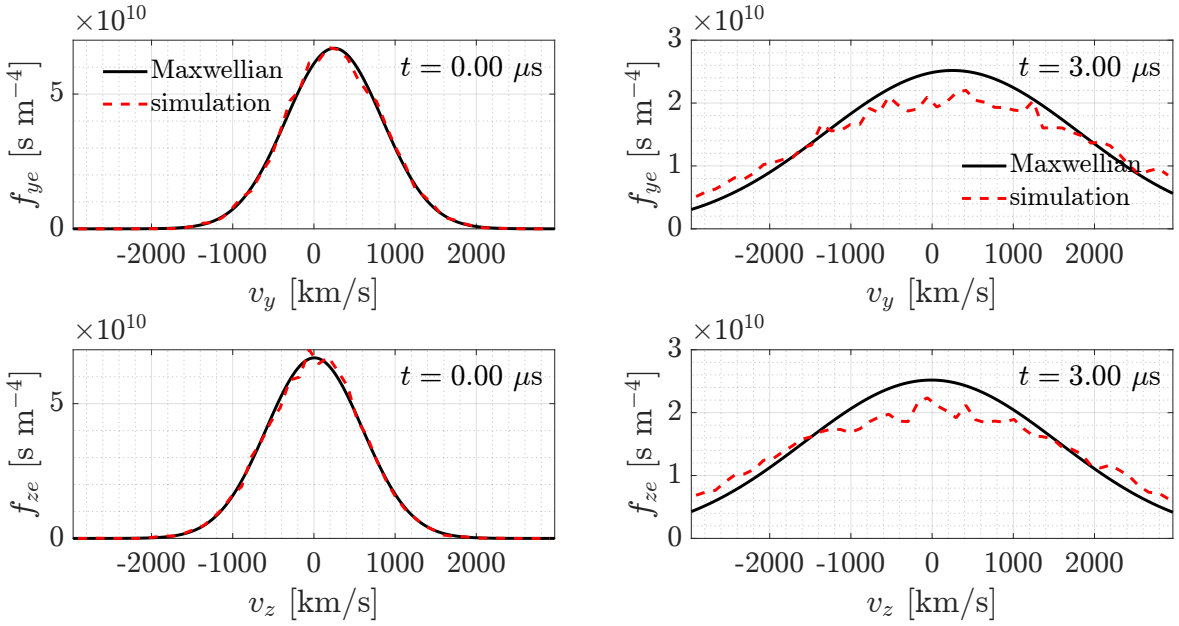

Fig. 7 Initial and final 1D-VDF of electrons in the (top) azimuthal and (bottom) axial directions. The initial Maxwellian VDF uses the equlibrium values $n_{e0} = 10^{17}$ m^{-3} and $T_e = 2$ eV. For later times, n_e and T_e from the simulations are used.

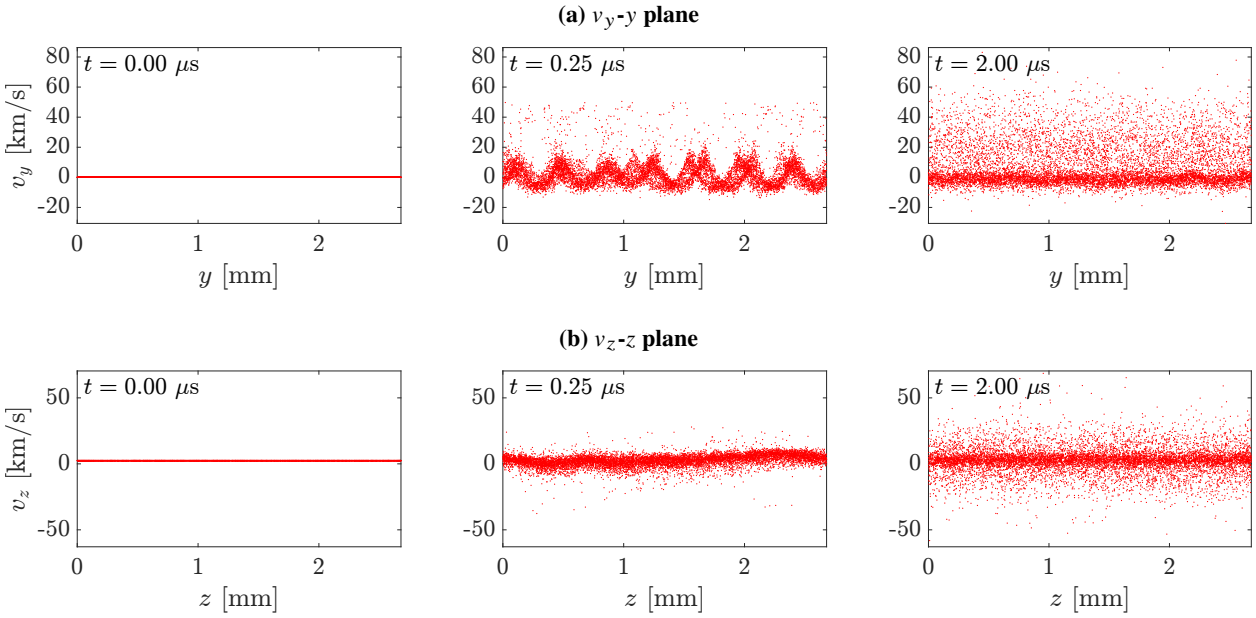

Fig. 8 Evolution of ion particles in the (a) v_y-y and (b) v_z-z plasnes of the phase space.

A. Spectral analysis

A simple determination of the characteristic frequency and wavelength of the ECDI oscillation, before saturation, can be done by inspection of figure 4. According to these results, the wave is mainly azimuthal with almost no axial propagation ($k_z = 0$). Although, there are minor 2D axial effects, 7 azimuthal wavelengths fit in the domain. This means that the obtained monochromatic wave corresponds to the mode number $n = 7$ ($\lambda_y = 0.38$ mm), that is close to

the resonance $m = 1$. The approximate frequency of the wave is $\omega_r = 60$ MHz and the phase velocity $\omega_r/k_y = 23$ km/s. The dominant wavelength coincide with the largest-γ mode predicted by the linear theory in figure 1, while linear results underestimate the wave frequency. However, in general, the long-term dominant modes in nonlinear simulation may not coincide with the most unstable modes in the linear dispersion relation [21]. For example, simulations (not included) with parameters based on reference [20] do not show such a good matching of simulations and linear results. As aforementioned, any comparison between the dispersion relation and simulations is challenging in the case of the ECDI since ω_r and γ are of the same order.

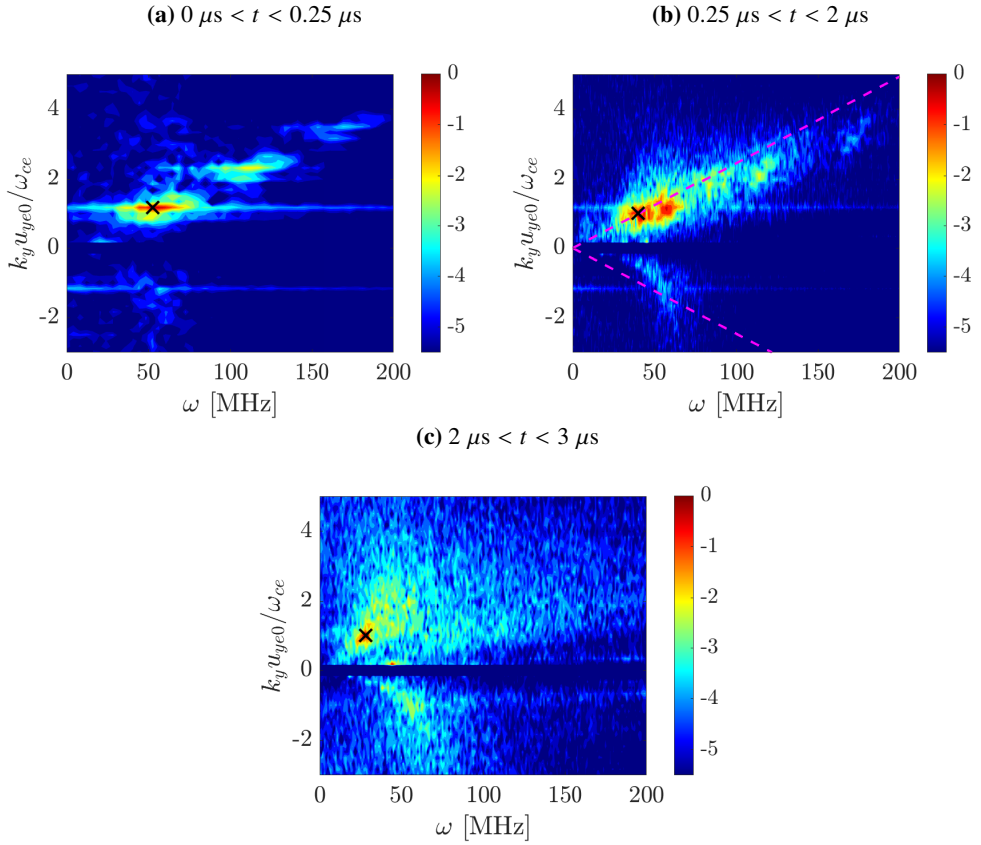

Fig. 9 Two-dimensional normalized fast Fourier transform of E_y at the fixed axial position $z = 5L_z/6$. The absolute maximum is marked with a black cross. In panel (b) the dispersion relation $\omega = \pm k_y c_s$ is plotted (magenta dashed line) for $T_e = 3.4$ eV.

A more detailed analysis of the frequency and wavenumber spectra of the results can be achieved via Fourier decomposition. Since the oscillations are main azimuthal, let us compute the two-dimensional Fourier transform of E_y in y and t for fixed $z = 5L_z/6$. To do so, we use three different time windows that correspond to the stages of the simulation seen in figure 3:

1) $0 < t < 0.25$ μs. The peaks seem to concentrate in bands near $k_y u_{ye0} = m\omega_{ce}$, that are the resonant terms in the dispersion relation 4. The maximum Fourier coefficient is located at $k_y u_{ye0} = 1.1667\omega_{ce}$ and $\omega_r = 52.4$ MHz. This is mode number $n = 7$, near $m = 1$, with a phase speed $\omega_r/k_y = 20$ km/s. There is secondary peak at $k_y u_{ye0} = 2.1667\omega_{ce}$ ($n = 13$, close to $m = 2$) and $\omega_r = 113$ MHz. The phase speed $\omega_r/k_y = 23$ km/s, that is similar to the main mode. The dominant wavelengths match the modes in the dispersion relation with the peaks in γ (see figure 1). As aforementioned, the linear results underestimate the frequency of oscillations observed in the simulations.

2) 0.25 μs $< t < 2$ μs. The bands of the spectrum at the resonant k_y have been blurred and there seems to be a linear

relation between k_y and ω_r. The peak in the spectrum is at the resonance $m = 1$, but its ω_r has been lowered to 40 MHz. The resultant phase speed is $\omega_r/k_y = 18$ km/s. This spectrum reminds of similar results reported in PIC simulations[23, 28] and experiments[4], where an ion-acoustic relation is proposed. In case of being an acoustic wave, it would correspond to an electron temperature of 3.4 eV. This value is, however, rather small compared with the temperature seen in the simulation in that interval. The acoustic dispersion relation $\omega = \pm k_y c_s$ for this T_e is represented in figure 9(b) for comparison. Let us note that the part of the spectrum for propagation in the $-\boldsymbol{E}_0 \times \boldsymbol{B}_0$ direction (this is $k_y < 0$) could correspond to the remnants of the counter-propagating ion-acoustic wave.

3) $2\ \mu\text{s} < t < 3\ \mu\text{s}$. Even if the peak still at $k_y u_{ye} = \omega_{ce}$, there is a mixing of different temporal and azimuthal scales and it is difficult to differentiate a clearly dominant mode in the spectrum. A clear acoustic-like dispersion relation is not observed anymore.

B. On energy conservation

Let us discuss in this section the conservation of total energy in the simulation domain for simulations of homogeneous plasma with periodic boundary conditions. The simulation discussed in this section does not have energy sources neither volumetric or through boundaries. Total energy integrated in the domain, accounting for particles and electric field energies, is expected to be conserved. This is, constant

$$\mathcal{E} = \int_V \left[\frac{1}{2}\varepsilon_0 E^2 + \frac{1}{2}(m_i n_i u_i^2 + m_e n_e u_e^2) + \frac{3}{2}(p_i + p_e) \right] \mathrm{d}V. \tag{7}$$

The work done by the electric field should act as mechanism that converts species energy on electric-field energy, and the other way around. However, a non-conventional feature of these simulations is that $\boldsymbol{E}$ and its work depends on the species. It can be proved that, for these conditions, the total energy changes according to

$$\frac{\partial \mathcal{E}}{\partial t} = \int_V (\boldsymbol{j}_e \cdot \boldsymbol{E}_0)\ \mathrm{d}V \tag{8}$$

where $\boldsymbol{j}_e = -e n_e \boldsymbol{u}_{ze}$ and $\mathcal{E}$ is defined as in equation (7) with $E = E_1$. Therefore, our simulation violates the conservation of energy. This was already suspected, looking at T_e, T_i and u_{yi} in figure 6. The plasma at the end of the simulation is much more energetic compared with the starting equilibrium. The evolution of the net average energy in the domain for electrons, ions and electric field is plotted in figure 10.

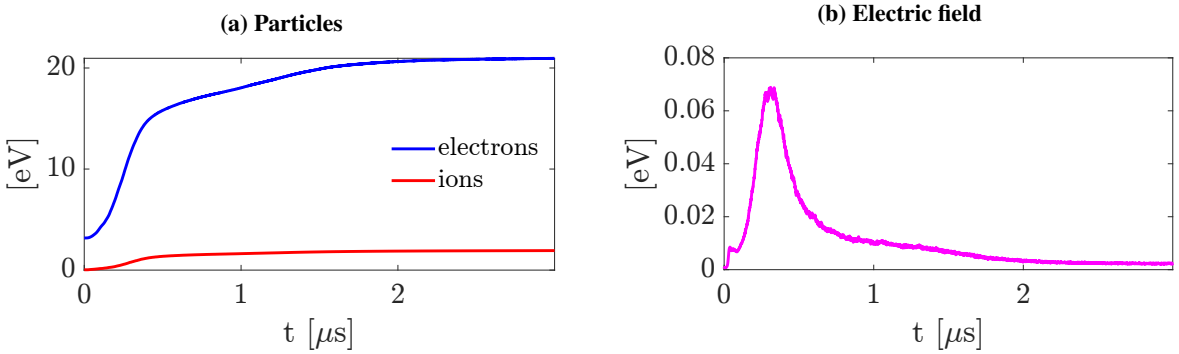

Fig. 10 Evolution of average energy of (a) particles and (b) electric field in the simulation domain.

C. Anomalous electron current

The simulation discussed in this section is collisionless, therefore there is no axial transport of electrons in the equilibrium conditions. If a non-zero current j_{ze} is observed in the axial direction, it is all an effect of the azimuthal plasma oscillations. The macroscopic momentum balance in the direction y for a magnetized electron flow, with negligible inertia and no collisions, yields

$$0 = e n_e E_y - B_0 j_{ze}; \tag{9}$$

with $n_e = n_{e0} + n_{e1}$. The usual relation[7] between j_{ze} and fluctutaions in density (n_{e1}) and azimuthal field (E_y) comes from isolating j_{ze} in the previous equation and computing the azimuthal average

$$\langle j_{ze} \rangle = \frac{e}{B_0} \langle n_{e1} E_y \rangle, \tag{10}$$

where the angle brackets stand for the average operation and $\langle n_{e0} E_y \rangle = 0$. Therefore, an axial cross-field transport is produced when there are a correlation between the azimuthal oscillations in E_y and n_{e1}.

In figure 11, $\langle j_{ze} \rangle$ is represented at axial position $z = 5L_z/6$. The blue solid line is the axial current observed in the simulation directly from the macroscopic properties of the electrons. The magenta broken line stands for $\langle j_{ze} \rangle$ calculated using equation 10. Both curves show the same trend and we can conclude the axial cross-field current is a result of the oscillations of n_{e1} and E_y. We see that some $\langle j_{ze} \rangle$ develops while the instability grows. After saturation the anomalous current is lost as oscillations in the plasma diminish.

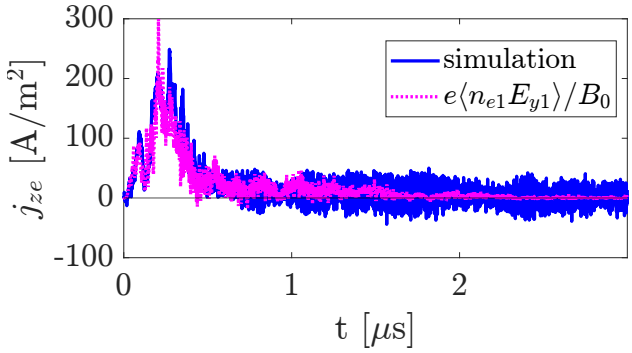

Fig. 11 Azimuthally averaged axial electron current at fixed axial position $z = 5L_z/6$. The value obtained from the volumetric weighting (solid blue) is compared with the anomalous current inferred from the correlation of oscillations in n_e and E_y (magenta broken).

V. ECDI simulation with injection conditions

In the previous section, we pointed out the possible interaction of particle injection or refreshing with the ECDI. To be precise, we suspected that the fact that plasma does not hold a sustained oscillation and an anomalous current may be related with the use of axial periodic conditions. Such conditions preserve the VDF of the particles resultant of interacting with the instability. When there is particle removal and injection/refreshing through boundaries, particles that have already interacted with the wave are removed from the simulation and new particles are injected having a different VDF that could possibly enhance the instability and lead to a sustained monochromatic oscillation.

Following this reasoning, a new simulation setup is presented here that replaces axial periodic conditions by injection surfaces. Periodic conditions are kept in the azimuthal direction. Any particle leaving the domain though axial boundaries is removed from the simulation. A constant flux of ions $g_{i0} = n_0 u_{zi0}$ is injected through the left boundary, with zero temperature and velocity $u_{zi0}\mathbf{1}_z$. A constant flux of electrons $g_{e0} = n_0 \bar{c}_{e0}/4$ is injected though left and right boundaries, whose velocities are sampled from a Maxwellian VDF with temperature T_{e0} and velocity $u_{ye0}\mathbf{1}_y$; being $\bar{c}_{e0} = \sqrt{8T_{e0}/\pi m_e}$. The value of g_{e0} is the flux produced by half a Maxwellian VDF. The injection fluxes are chosen such that they match the amount of ions and electrons leaving the domain in equilibrium conditions.

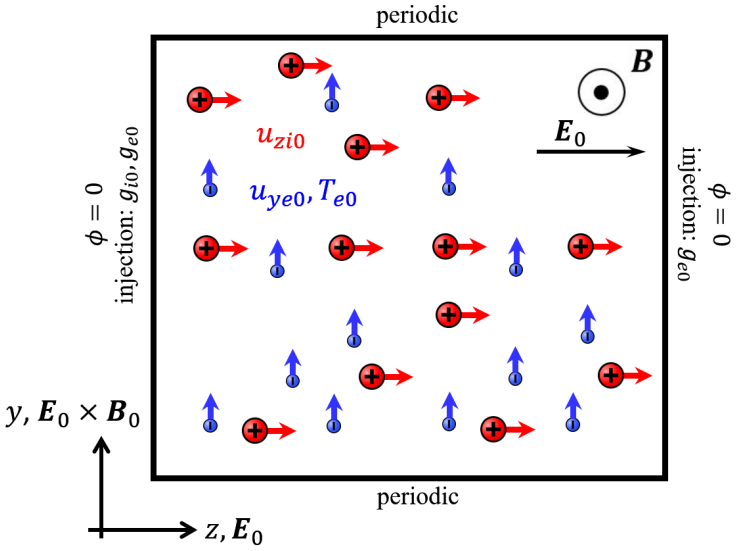

Fig. 12 Diagram summarizing the simulation axes, boundary conditions and initial equilibrium state for the ECDI simulation with axial plasma injection.

Once the instability arises, the injected fluxes do not need to coincide with fluxes leaving the domain and the number of particles in the simulation may change. Moreover, the number of ions and electrons may not coincide so that the domain could have a net non-zero charge. For that reason, axial conditions on potential are also changed from periodic to fixed potential $\phi = 0$. The finite-difference version of the Poisson solver is used. The new boundary conditions are equivalent to the periodic ones in the equilibrium state. The new simulation configuration is summarized in figure 12.

Other than different boundary conditions, the parameters for the first simulation of this section are the same as in section (IV). The evolution of E_y is represented in figure 13. Up to $t = 0.15$ μs, the behavior is similar to the periodic case of figure 3 and we see the growth of a quite monochromatic wave, with minor differences such as an small non-zero k_z. In frames $t = 0.25$ μs and $t = 0.5$ μs, the oscillation seem to move far from the injection surface of ions. For later times, the oscillation level decrease, although there are some remnants of the initial oscillation frames $t = 2.5$ μs and $t = 3.0$ μs.

Even if the initial monochromatic oscillation seem to be more persistent in this case, compared with periodic conditions, a sustained oscillation was not reached. In previous section, we saw a significant interaction of ions with the electrostatic wave in the form of ion-wave trapping. Ions seem to play, thus, an important role in the growth and saturation of the ECDI. The residence time of ions, estimated with the equilibrium velocity, is $\Delta t_{i0} = L_z/u_{zi0} = 1.1$ μs. On the other hand, from previous section, the saturation time of the instability is, approximately, $\Delta t_{\text{sat}} = 0.3$ μs. The limit $\Delta t_{i0} \gg \Delta t_{\text{sat}}$ corresponds to the periodic simulation of the previous section. In the opposite limit, $\Delta t_{i0} \ll \Delta t_{\text{sat}}$, we do not see a sustained oscillation (case not included in the article), since ions do not have time to interact with the wave. According to this reasoning, we could expect a sustained oscillation in the intermediate regime where Δt_{i0} is similar to Δt_{sat}. Following this line of thinking, a similar simulation has been performed increasing the ion velocity to $u_{zi0} = 5$ km/s, and modifying the injection flux accordingly. This new u_{zi0} yields $\Delta t_{i0} = 0.50$ μs, that is closer to Δt_{sat}.

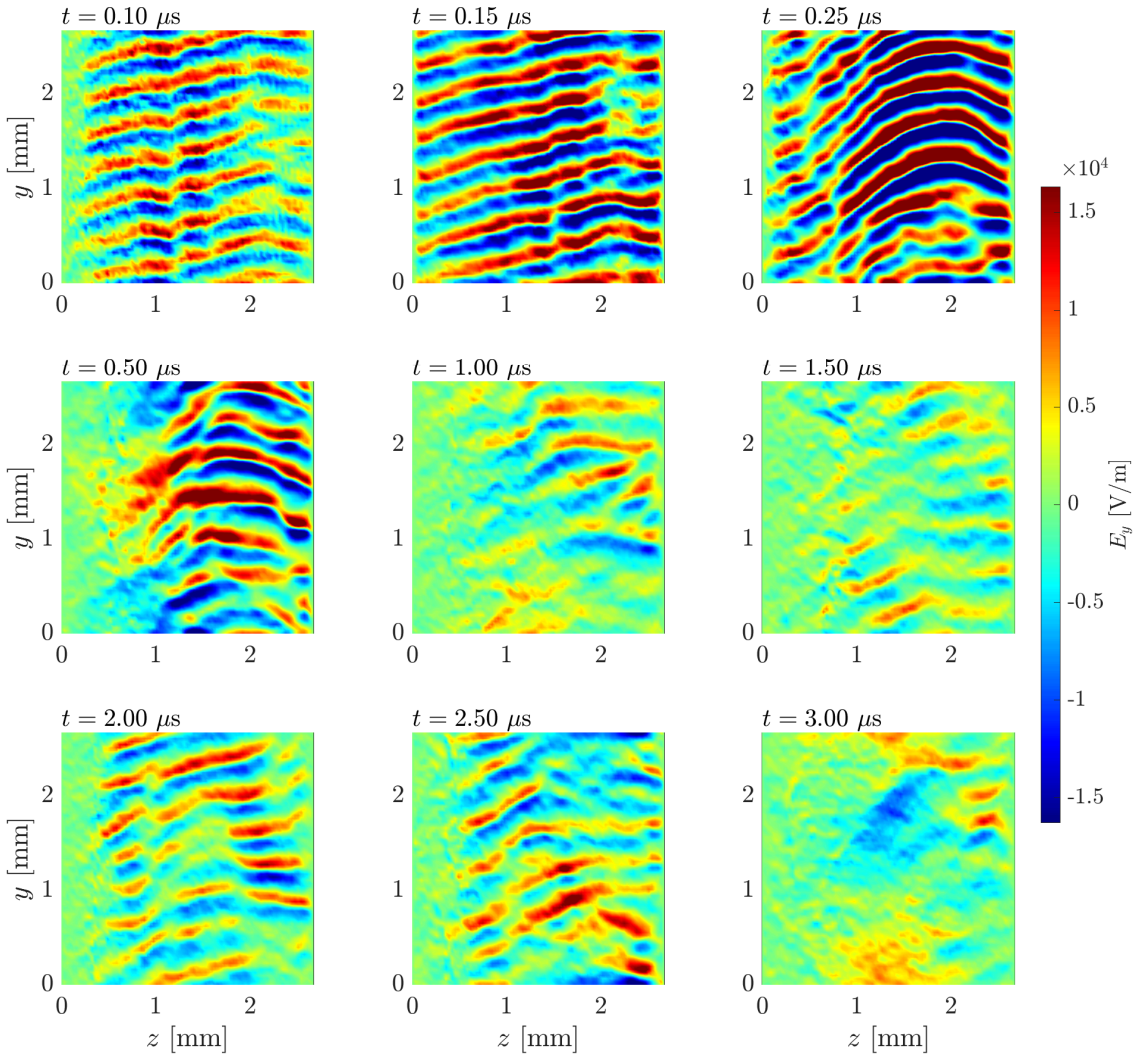

Fig. 13 Time evolution of E_y in the yz-plane, for axial injection conditions and ion residence time $\Delta t_{i0} = 1.1$ μs.

The evolution of E_y in figure 14 for times before 0.5 μs is practically the same as for the case of figure 13. That is, the initial instability formation and saturation. However, after 0.5 μs we can see a second saturation and the formation of a nearly monochromatic wave that develops at some distance from the ion injection surface. It has been checked that this wave survive also for longer times. Other characteristic of this long-terms oscillation is that the wavefronts have some curvature (meaning different axial propagation depending on the axial position). A similar feature is observed in some 2D-yz simulations of the Hall discharge [23, 28] close to the exit, where the maximum magnetic field takes place. Here, however, the used radial $\boldsymbol{B}_0$ is uniform in the whole domain. This phenomena has to be further investigated.

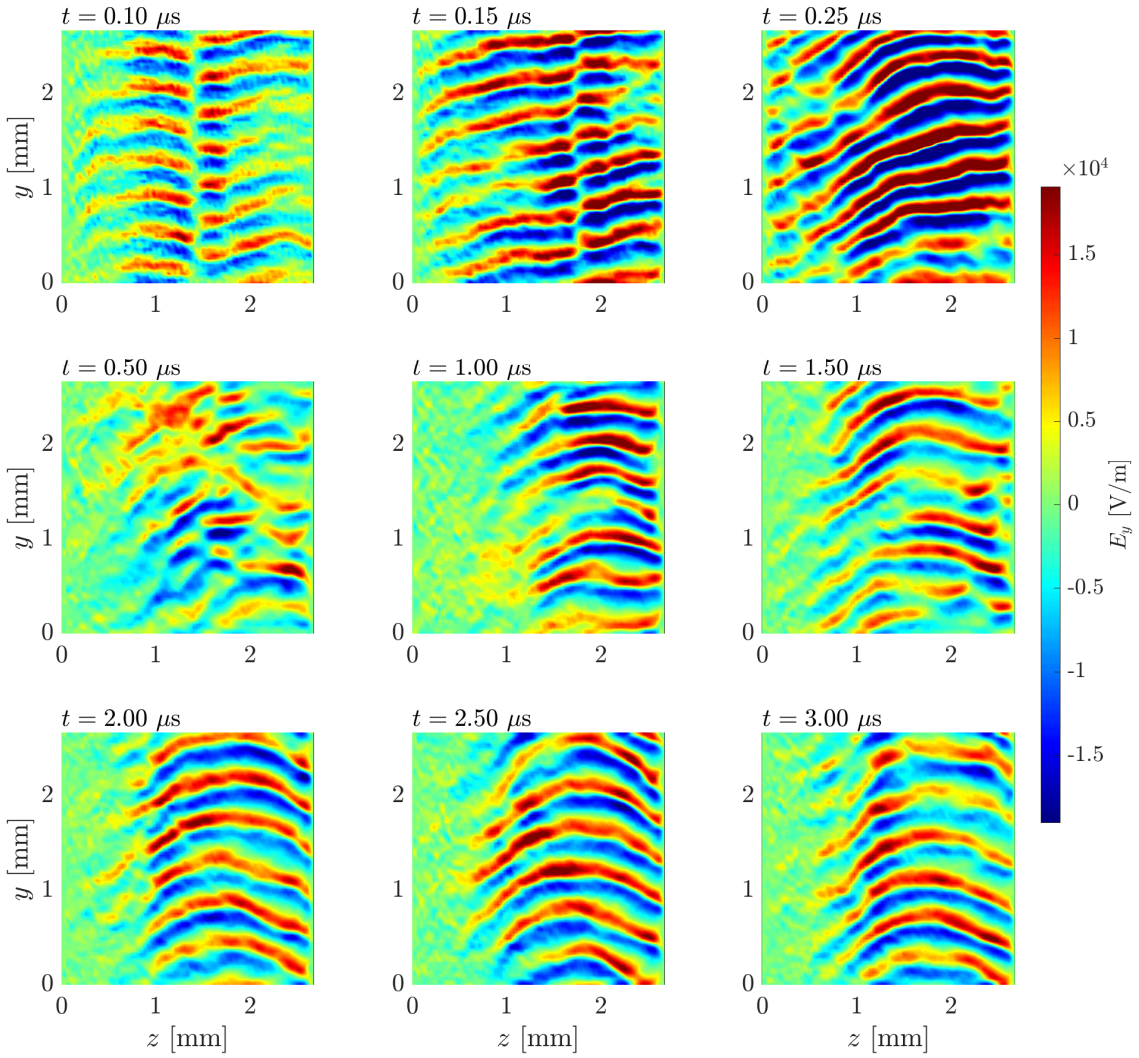

Fig. 14 Time evolution of E_y in the yz-plane, for axial injection conditions and ion residence time $\Delta t_{i0} = 0.5$ μs.

To summarize, as it was suggested, the formation of a stationary oscillation seems to be related to the residence time of ions and how it compares with the characteristic saturation time. Depending on that, several regimes are identified and the one leading to a stationary monochromatic oscillation is $\Delta t_{i0} \sim \Delta t_{\text{sat}}$. This is the regime interesting from the point of view of electron anomalous transport, which is discussed later.

Before moving to the analysis of the Fourier spectrum and cross-field transport, let us comment on the electron heating. In the periodic simulation (see figure 6), a significant electron heating was observed from 2 eV to 14 eV at the end of the simulation. In the case with injection (figure 15), electrons with $T_e = 2$ eV are continuously injected through axial boundaries. Also, hotter electrons heated by the ECDI are removed when they reach the injection boundaries. The final electron population satisfies the 2 eV temperature close to the injection surfaces, while the ECDI oscillation heats them in the central part of the domain. However, the final temperatures are significantly lower than in the periodic case. The average temperature at the middle axial location is about 4 eV. The electron heating can be also seen in the broadening of the electron 1D-VDFs, in figure 16, measured in central point. The distribution functions seem flattened close to the average velocity, departing from the corresponding Maxwellian (with n_e and T_e from the simulation).

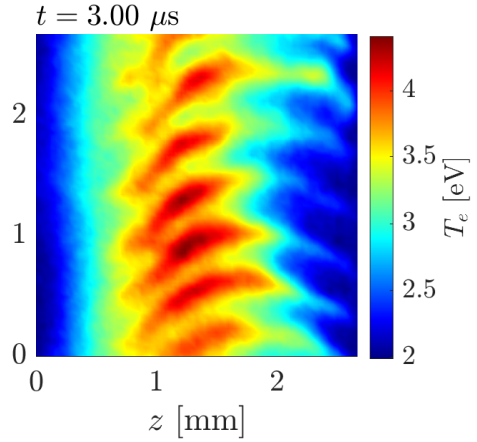

Fig. 15 T_e **at the end of the simulation, for the case with** $\Delta t_{i0} = 0.5\ \mu$**s.**

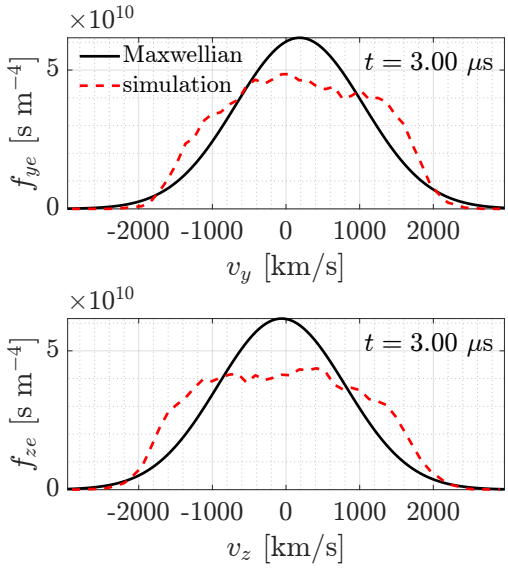

Fig. 16 1D-VDFs of electrons at the end of the simulation measured at central point of the domain, for the case with $\Delta t_{i0} = 0.5\ \mu$**s.**

A. Spectral analysis

The two-dimensional Fourier transform is computed in figure 17 for the same time windows as in the periodic simulation. The spectrum for times before 0.25 μs is similar to what already observed. The discrete behavior at the resonant scales $k_y u_{ye0} = m\omega_{ce}$ are, however, not so marked as in panel (a) of figure 9. For times between 0.25 and 2 μs, the spectrum suggest again an ion-acoustic-like dispersion relation. For later times, the spectrum is much more clean than 9(c), where there is significant mix of scales. In this case, there is a clear dominant mode in the long-term with $\omega_r = 48$ MHz and $\lambda_y = 0.44$ mm ($m = 1$, $n = 6$), that is also close to the peaks for earlier times. The phase speed of this wave is $\omega_r/k_y = 21$ km/s. Following the interpretation of the ion-acoustic mode, these results suggest a sound wave with an electron temperature of 4.6 eV, that is surprisingly close to T_e observed in the central part of figure 15. In every time interval, the simulation spectra show an excellent matching with the acoustic dispersion relation. Also in the $k_y < 0$ part of the spectrum.

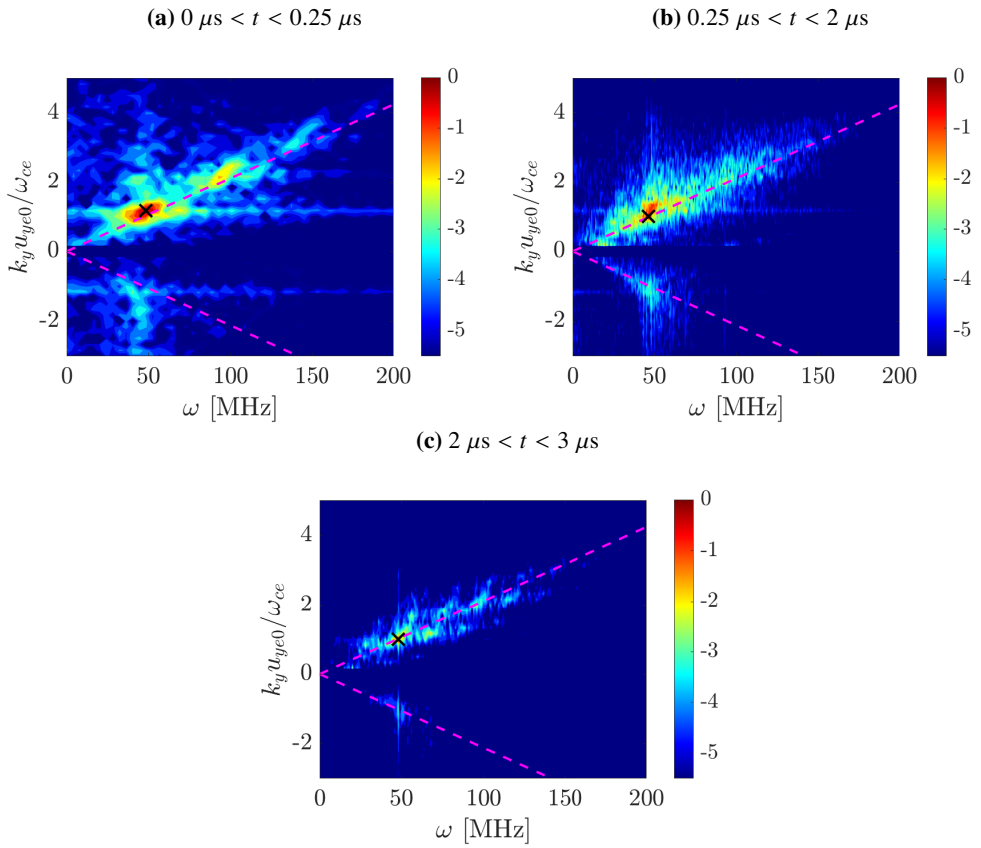

Fig. 17 Logarithm of the two-dimensional normalized fast Fourier transform of E_y, in y and t with fixed $z = 5L_z/6$. For the case with $\Delta t_{i0} = 0.5$ μs. The dispersion relation $\omega = \pm k_y c_s$ is plotted (magenta dashed line) for $T_e = 4.6$ eV.

B. Anomalous electron current

The calculation of $\langle j_{ze} \rangle$ is repeated here, comparing values directly measured in the simulation and the current inferred from fluctuations. The results in figure 18 show an initial peak in the current, similarly to the periodic case in 11. However, the formation of an azimuthal wave that survives long simulation times leads to a stationary axial cross-field transport of electrons, produced by oscillations. This result is of interest for the case of Hall-thruster discharges, where we expect there is a sustained contribution from azimuthal fluctuations to the axial transport.

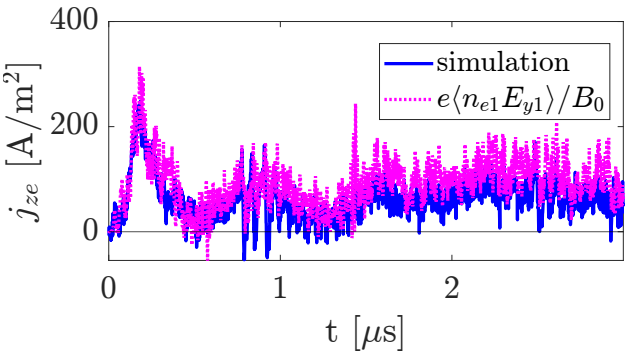

Fig. 18 Azimuthally averaged axial electron current, for the case with $\Delta t_{i0} = 0.5$ μs.

VI. Conclusion

In this paper, we present a recently developed 2D electrostatic PIC model that is intended to simulate diverse plasma discharge scenarios. One of the primary intents of this code is the simulation and study of plasma instabilities and turbulent transport in the Hall-thruster discharge and other $\boldsymbol{E}_0 \times \boldsymbol{B}_0$ plasmas. To be precise, we have focused here on axial-azimuthal instabilities. One of the instabilities that have been calling the attention of the electric propulsion community is the electron cyclotron drift instability that takes place in plasmas with magnetized electrons and unmagnetized ions that hold a large relative drift, when accounting for kinetic effects on the electrons. The linear theory of the ECDI predicts unstable waves close to the resonances of the electron Doppler shift with the cyclotron harmonics.

For this work, we propose the simulation of a simplified scenario that gets as close as possible to the assumptions behind the linear ECDI theory, removing many complex effects accounted for in Hall-thurster-like simulations. To do so, an initially homogeneous plasma is simulated with periodic boundary conditions in every direction and ignoring collisional effects. In order to comply with the hypotheses of the ECDI dispersion relation, electrons are moved according to $\boldsymbol{B}_0$ and $\boldsymbol{E}_0 + \boldsymbol{E}_1$ fields; while electrons only react to the oscillating part $\boldsymbol{E}_1$ of the electric field. Using an electric field that depends on the species leads to the violation of the energy conservation. For these conditions, the ECDI manifest and a monochromatic wave can be distinguished before saturation, that is effective in producing an anomalous electron transport. Ions experience wave trapping and seem to play an important role in the instability formation and saturation. After saturation, there is significant mixing of modes but the Fourier spectrum shows an ion-acoustic-like dispersion relation. For long simulation times, oscillations tends to get diminished and there is no axial electron current.

A second set of simulations is proposed, where axial periodic conditions are substituted by injection conditions with a fixed potential. Moreover, any particle crossing these boundaries is removed from the simulation. Injection conditions are chosen such that the initial plasma state is an equilibrium equivalent to the previous periodic simulations. Different behaviors are observed depending on the size of the residence ion time relative to the saturation time. It is found that, when these two are similar, an stationary monochromatic oscillation forms at some distance from the ion inlet boundary that produces a sustained axial transport of electrons. These results suggest that ion injection have a strong influence on the long-term behavior of the ECDI. This matter will be further investigated and is expected to help to the understanding of more realistic Hall-thruster simulations.

Acknowledgments

This research was funded by the ESPEOS project, funded by the Agencia Estatal de Investigación (Spain's National Research and Development Plan), under Grant No.PID2019-108034RB-I00/AEI/10.13039/501100011033. Additional support came from Comunidad de Madrid (Spain), under PROMETEO-CM project, with Grant No. Y2018/NMT-4750. Enrique Bello-Benítez is supported by Spain's Ministerio de Ciencia, Innovación y Universidades, under Grant No. FPU18/03686. The authors acknowledge useful discussions on this work with A. Domínguez-Vazquez, P. Fajardo and M. Merino.

References

[1] Choueiri, E., and Ziemer, J., "Quasi-steady magnetoplasmadynamic thruster performance database," *Journal of Propulsion and Power*, Vol. 17, No. 5, 2001, pp. 967–976.

[2] Ellison, C., Raitses, Y., and Fisch, N., "Cross-field electron transport induced by a rotating spoke in a cylindrical Hall thruster," *Physics of Plasmas*, Vol. 19, No. 1, 2012, p. 013503.

[3] MacDonald, N. A., Cappelli, M. A., Gildea, S. R., Martinez-Sanchez, M., and Hargus Jr, W. A., "Laser-induced fluorescence velocity measurements of a diverging cusped-field thruster," *Journal of Physics D: Applied Physics*, Vol. 44, No. 29, 2011, p. 295203.

[4] Tsikata, S., Lemoine, N., Pisarev, V., and Gresillon, D., "Dispersion relations of electron density fluctuations in a Hall thruster plasma, observed by collective light scattering," *Physics of Plasmas*, Vol. 16, 2009, p. 033506.

[5] Tsikata, S., and Minea, T., "Modulated electron cyclotron drift instability in a high-power pulsed magnetron discharge," *Physical Review Letters*, Vol. 114, 2015, p. 185001.

[6] Tsikata, S., Héron, A., and Honoré, C., "Hall thruster microturbulence under conditions of modified electron wall emission," *Physics of Plasmas*, Vol. 24, No. 5, 2017, p. 053519. https://doi.org/10.1063/1.4984255, URL ttps://doi.org/10.1063/1.4984255.

[7] Janes, G., and Lowder, R., "Anomalous electron diffusion and ion acceleration in a low-density plasma," *Physics of Fluids*, Vol. 9, No. 6, 1966, pp. 1115–1123.

[8] Bello-Benítez, E., and Ahedo, E., "Axial-azimuthal, high-frequency modes from global linear-stability model of a Hall thruster," *Plasma Sources Science and Technology*, Vol. 30, No. 3, 2021, p. 035003. https://doi.org/10.1088/1361-6595/abde21.

[9] Ramos, J. J., Bello-Benítez, E., and Ahedo, E., "Local analysis of electrostatic modes in a two-fluid E x B plasma," *Physics of Plasmas*, Vol. 28, No. 5, 2021, p. 052115. https://doi.org/10.1063/5.0039341, URL https://doi.org/10.1063/5.0039341.

[10] Koshkarov, O., Smolyakov, A., Raitses, Y., and Kaganovich, I., "Self-Organization, Structures, and Anomalous Transport in Turbulent Partially Magnetized Plasmas with Crossed Electric and Magnetic Fields," *Physical Review Letters*, Vol. 122, 2019, p. 185001. https://doi.org/10.1103/PhysRevLett.122.185001, URL https://link.aps.org/doi/10.1103/PhysRevLett.122.185001.

[11] Frias, W., Smolyakov, A., Kaganovich, I., and Raitses, Y., "Long wavelength gradient drift instability in Hall plasma devices. I. Fluid theory," *Physics of Plasmas*, Vol. 19, 2012, p. 072112.

[12] Nikitin, V., Tomilin, D., Lovtsov, A., and Tarasov, A., "Gradient-drift and resistive mechanisms of the anomalous electron transport in Hall effect thrusters," *Europhysics Letters*, Vol. 117, No. 4, 2017, p. 45001.

[13] Sorokina, E. A., Marusov, N. A., Lakhin, V. P., and Ilgisonis, V. I., "Discharge Oscillations in Morozov's Stationary Plasma Thruster as a Manifestation of Large-Scale Modes of Gradient Drift Instability," *Plasma Physics Reports*, Vol. 45, No. 1, 2019, p. 1.

[14] Romadanov, I., Smolyakov, A., Raitses, Y., Kaganovich, I., Tian, T., and Ryzhkov, S., "Structure of nonlocal gradient-drift instabilities in Hall ExB discharges," *Physics of Plasmas*, Vol. 23, 2016, p. 122111.

[15] Forslund, D., Morse, R., and Nielson, C., "Electron cyclotron drift instability," *Physical Review Letters*, Vol. 25, 1970, pp. 1266–1270.

[16] Wong, H., "Electrostatic electron-ion streaming instability," *Physics of Fluids*, Vol. 13, 1970, pp. 757–760.

[17] Adam, J., Herón, A., and Laval, G., "Study of stationary plasma thrusters using two-dimensional fully kinetic simulations," *Physics of Plasmas*, Vol. 11, 2004, pp. 295–305.

[18] Ducrocq, A., Adam, J., Héron, A., and Laval, G., "High-frequency electron drift instability in the cross-field configuration of Hall thrusters," *Physics of Plasmas*, Vol. 13, 2006, p. 102111.

[19] Cavalier, J., Lemoine, N., Bonhomme, G., Tsikata, S., Honoré, C., and Grésillon, D., "Hall thruster plasma fluctuations identified as the ExB electron drift instability: Modeling and fitting on experimental data," *PoP*, Vol. 20, No. 8, 2013, p. 082107.

[20] Lafleur, T., Baalrud, S., and Chabert, P., "Theory for the anomalous electron transport in Hall effect thrusters. II. Kinetic model," *Physics of Plasmas*, Vol. 23, 2016, p. 053503.

[21] Janhunen, S., Smolyakov, A., Sydorenko, D., Jimenez, M., Kaganovich, I., and Raitses, Y., "Evolution of the electron cyclotron drift instability in two-dimensions," *Physics of Plasmas*, Vol. 25, No. 8, 2018, p. 082308.

[22] Lafleur, T., Baalrud, S., and Chabert, P., "Theory for the anomalous electron transport in Hall effect thrusters. I. Insights from particle-in-cell simulations," *Physics of Plasmas*, Vol. 23, 2016, p. 053502.

[23] Lafleur, T., and Chabert, P., "The role of instability-enhanced friction on 'anomalous' electron and ion transport in Hall-effect thrusters," *Plasma Sources Science and Technology*, Vol. 27, 2017, p. 015003.

[24] Coche, P., and Garrigues, L., "A two-dimensional (azimuthal-axial) particle-in-cell model of a hall thruster," *Physics of Plasmas*, Vol. 21, 2014, p. 023503.

[25] Janhunen, S., Smolyakov, A., Chapurin, O., Sydorenko, D., Kaganovich, I., and Raitses, Y., "Nonlinear structures and anomalous transport in partially magnetized ExB plasmas," *Physics of Plasmas*, Vol. 25, 2018, p. 11608.

[26] Asadi, Z., Taccogna, F., and Sharifian, M., "Numerical Study of Electron Cyclotron Drift Instability: Application to Hall Thruster," *Frontiers in Physics*, Vol. 7, 2019. https://doi.org/10.3389/fphy.2019.00140, URL https://www.frontiersin.org/article/10.3389/fphy.2019.00140.

[27] Adam, J., Boeuf, J., Dubuit, N., Dudeck, M., Garrigues, L., Gresillon, D., Heron, A., Hagelaar, G., Kulaev, V., Lemoine, N., et al., "Physics, simulation and diagnostics of Hall effect thrusters," *Plasma Physics and Controlled Fusion*, Vol. 50, 2008, p. 124041.

[28] Charoy, T., Boeuf, J. P., Bourdon, A., Carlsson, J. A., Chabert, P., Cuenot, B., Eremin, D., Garrigues, L., Hara, K., Kaganovich, I. D., Powis, A. T., Smolyakov, A., Sydorenko, D., Tavant, A., Vermorel, O., and Villafana, W., "2D axial-azimuthal particle-in-cell benchmark for low-temperature partially magnetized plasmas," *Plasma Sources Science and Technology*, Vol. 28, No. 10, 2019, p. 105010.